

# CATNet: Collaborative Alignment and Transformation Network for Cooperative Perception

Gong Chen<sup>1</sup> Chaokun Zhang<sup>2\*</sup> Tao Tang<sup>1</sup> Pengcheng Lv<sup>3</sup> Feng Li<sup>1</sup> Xin Xie<sup>1</sup>

<sup>1</sup>School of Computer Science and Technology, Tianjin University

<sup>2</sup>School of Cybersecurity, Tianjin University <sup>3</sup>School of Future Technology, Tianjin University

## Abstract

Cooperative perception significantly enhances scene understanding by integrating complementary information from diverse agents. However, existing research often overlooks critical challenges inherent in real-world multi-source data integration, specifically high temporal latency and multi-source noise. To address these practical limitations, we propose Collaborative Alignment and Transformation Network (CATNet), an adaptive compensation framework that resolves temporal latency and noise interference in multi-agent systems. Our key innovations can be summarized in three aspects. First, we introduce a Spatio-Temporal Recurrent Synchronization (STSync) that aligns asynchronous feature streams via adjacent-frame differential modeling, establishing a temporal-spatially unified representation space. Second, we design a Dual-Branch Wavelet Enhanced Denoiser (WTDen) that suppresses global noise and reconstructs localized feature distortions within aligned representations. Third, we construct an Adaptive Feature Selector (AdpSel) that dynamically focuses on critical perceptual features for robust fusion. Extensive experiments on multiple datasets demonstrate that CATNet consistently outperforms existing methods under complex traffic conditions, proving its superior robustness and adaptability.

## 1. Introduction

Accurate environmental perception is paramount for the reliability of autonomous driving systems, as it directly influences downstream decision-making and control [22]. However, single-agent perception systems inherently face limitations due to restricted fields of view and prevalent occlusion phenomena. These constraints pose significant challenges [5, 9, 34] in maintaining robust perception capabilities within large-scale scenarios. To overcome these constraints, multi-agent cooperative perception [10, 29, 30] has emerged as a critical technological paradigm. By lever-

\*Corresponding author.

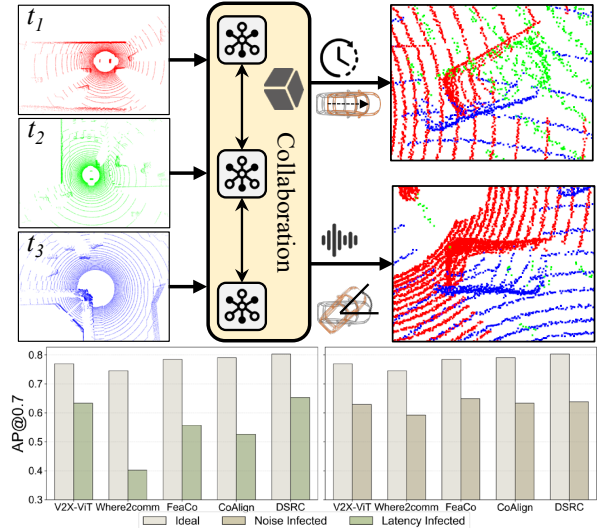


Figure 1. Schematic of cooperative perception under latency and noise.

aging Vehicle-to-Everything (V2X) communication infrastructures to achieve distributed information fusion, it has become a prominent research focus in the field.

Although numerous studies [28, 29, 31] have demonstrated promising results through feature interaction modeling under ideal communication assumptions, their practical effectiveness in dynamic real-world environments [6] remains constrained. Specifically, inter-agent communications are vulnerable to channel interference and transmission noise [23], leading to feature distortion in vehicular perception data. Existing methods struggle to reconstruct spatio-temporally consistent perceptual representations [35], resulting in substantial performance degradation. The fundamental challenges can be attributed to two critical issues:

**Time-Varying Communication Latency.** Dynamic latency poses a significant threat to system robustness by disrupting the spatio-temporal coherence between features from the ego-vehicle and its collaborators. As illustrated

in the top-right panel of Figure 1, features from different timestamps are misaligned due to transmission delays. This misalignment creates ghosting artifacts and feature fragmentation, fundamentally compromising perception consistency. The severity of this issue is quantified in our analysis (Figure 1, bottom-left bar chart), where latency leads to a performance drop of up to 46%. While prior solutions [11, 33] typically perform local temporal alignment on individual agent features before fusion, these frameworks prove insufficient as they inadequately leverage global spatio-temporal context.

**Noise-Induced Feature Degradation.** Features in cooperative perception are susceptible to corruption from multi-source noise during transmission. This degradation is exacerbated under asynchronous conditions, where coupled interference effects severely impact the pipeline. As depicted in the bottom-right panel of Figure 1, noise deteriorates the geometric structure of the point cloud, introducing spurious artifacts and significant distortion of object shapes. This detrimental effect is confirmed in the bar chart, where noise pollution causes a performance drop of up to 17%. Existing methods primarily focus on geometry-based registration [14, 21, 27] or fixed-threshold denoising [12, 24]. They either fail to adequately correct for systematic errors or inadvertently suppress crucial discriminative features, leading to suboptimal outcomes.

To address these challenges, we propose Collaborative Alignment and Transformation Network (**CATNet**), a dynamic adaptive compensation framework. It effectively tackles robust collaboration in multi-agent systems through the ingenious integration of three novel modules. To handle spatio-temporal misalignment, we design a Spatio-Temporal Recurrent Synchronization (**STSync**) module. It establishes a global temporal context by recurrently propagating the ego-vehicle’s features to iteratively align asynchronous data streams. Subsequently, to resolve the feature degradation caused by amplified noise and feature inconsistencies, we devise a purification strategy with next two modules. At the signal level, we design a Dual-Branch Wavelet Enhanced Denoiser (**WTDen**) module, which corrects global distortions with a Wavelet Mamba and remedies local inconsistencies via Wavelet Convolution. Subsequently, at the semantic level, we design a Adaptive Feature Selector (**AdpSel**) module to refine collaborative features by selecting critical regions and pruning artifacts, ensuring the robustness of the final fusion.

To validate the effectiveness of CATNet, we conducted extensive experiments on various cooperative perception datasets. Using the V2XSet as an example, results demonstrate that our method achieves an average AP@0.5/AP@0.7 improvement of 5.7%/2.5% compared to the second-best approach, and outperforms the single-vehicle baseline by 16.0%/12.7% under noisy and latency

scenarios. Our contributions can be summarized as follows.

- We propose CATNet, a novel cooperative perception framework specifically engineered to overcome two fundamental challenges in multi-agent systems: communication asynchrony and feature inconsistency.
- We design STSync for robust temporal alignment and introduce a dual-purification strategy that uses WTDen for signal denoising and AdpSel for semantic refinement.
- We conduct extensive experiments on large-scale datasets, demonstrating that CATNet achieves state-of-the-art performance and shows remarkable robustness, especially under severe communication delays and noise.

## 2. Related Work

**Cooperative Perception.** Cooperative perception technology enhances the environmental sensing capabilities [27, 29, 36] of individual agents [39, 40] through information sharing among multiple agents, and has become a research hotspot in autonomous driving and multi-robot systems. Mainstream research methods are divided into three categories. Early fusion [1, 4] integrates information at the raw data level, achieving global perception by sharing point cloud or image data, but it imposes stringent requirements on communication bandwidth. Late fusion [25, 36] occurs at the individual decision-making level, but it is limited by the local perception capabilities of individual agents and suffers from significant information loss, making it difficult to handle occlusions or distant targets. Intermediate fusion [28, 29, 32] facilitates information exchange at the feature level, enabling efficient collaboration through the sharing of intermediate feature maps. This approach has become the most prominent technical paradigm in the field, and many studies have achieved promising results in terms of perception accuracy. However, current intermediate fusion methods remain vulnerable in complex environments with heterogeneous noise profiles and dynamic latency.

**Multi-Agent Latency Mitigation.** Cooperative perception systems face asynchronous feature misalignment during fusion due to transmission delays and communication interruptions [7]. Current solutions primarily adopt two strategies: Methods like V2X-ViT [28] and V2VNet [27] concatenate asynchronous features and implicitly learn spatio-temporal correlations through deep networks, but fail to capture dynamic scene evolution, while alignment-focused approaches such as SyncNet [16] (using P-LSTM for timestamp synchronization) and MRCNet [11] (employing feature prediction networks) attempt local compensation but lack global spatio-temporal coherence modeling across agents. These limitations lead to incomplete predictions and iterative error accumulation, as neither paradigm effectively addresses multi-agent temporal consistency or prevents error propagation through collaborative processing chains.

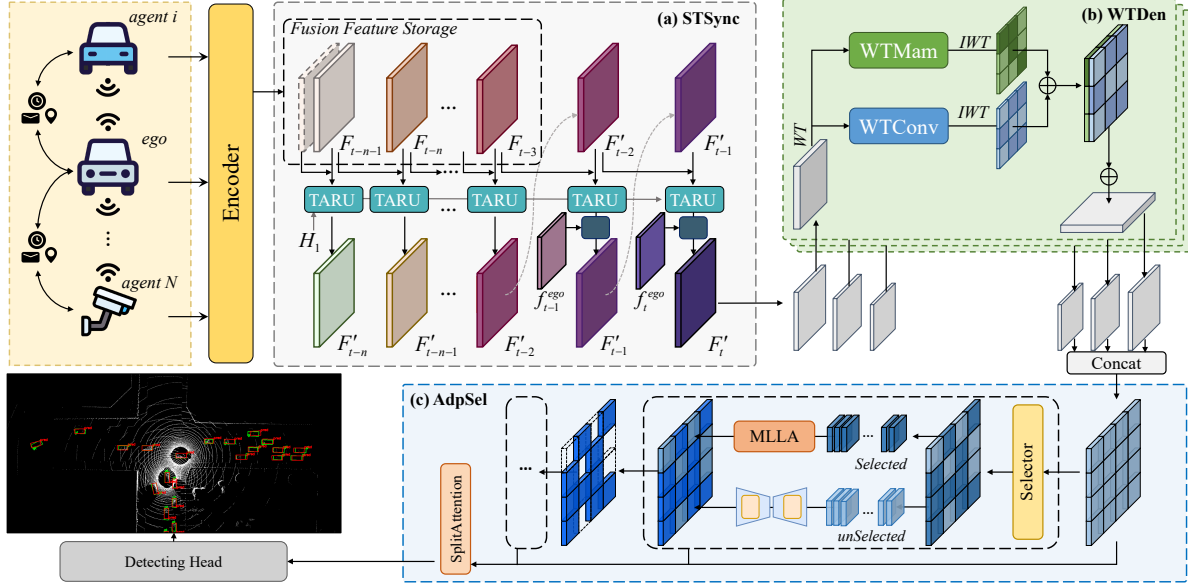


Figure 2. Architectural overview of the CATNet framework. The ego vehicle maintains a fusion feature bank that processes multi-agent transmitted features, employing temporal prediction mechanisms for current-time feature estimation. These refined features subsequently undergo denoising operations and salient feature extraction, achieving robust cross-agent feature fusion via learnable aggregation weights.

**Multi-Source Noise Suppression.** Cooperative perception systems suffer from multi-source noise, including sensing inaccuracies, communication distortions, model deviations, and latency artifacts across the pipeline [2, 3]. Current solutions primarily adopt two paradigms: knowledge distillation and graph optimization. The first approach, represented by DiscoNet [19] and DI-V2X [18], employs teacher-student frameworks to suppress interference through clean feature guidance, yet exhibits critical limitations including teacher model dependency and inadequate performance in compounded interference scenarios. The second paradigm exemplified by CoAlign [21] utilizes graph-based spatial alignment to correct sensor distortions, but suffers from temporal inconsistency in dynamic environments where communication delays induce asynchronous feature misalignment and cascading errors. However, a key limitation persists: existing methods primarily purify features at a signal level, while overlooking residual semantic inconsistencies and contextual artifacts. This incomplete approach to purification critically undermines system reliability.

### 3. Methods

#### 3.1. Overall Architecture

To address the dual challenges of non-deterministic transmission delays and multi-source noise interference in cooperative perception scenarios, we propose a Collaborative Alignment and Transformation Network (CATNet). The complete workflow comprises four components: a fea-

ture encoder, feature transmission, CATNet, and a feature decoder. Our framework operates through the following pipeline:

$$F_i^t = f_{\text{encoder}}(X_i^t), \quad i \in N \quad (1)$$

$$\hat{F}_{i \rightarrow \text{ego}}^{t-\tau} = \xi_{i \rightarrow \text{ego}}^{t-\tau}(F_i^{t-\tau}) \quad (2)$$

$$\tilde{F}_{\text{fused}}^t = \text{CATNet}\left(\left\{\hat{F}_{i \rightarrow \text{ego}}^{t'}\right\}_{t' \leq t-\tau}, \left\{F_{\text{ego}}^{t'}\right\}_{t' \leq t}\right) \quad (3)$$

$$\tilde{Y}_{\text{fused}}^t = f_{\text{decoder}}\left(\tilde{F}_{\text{fused}}^t\right) \quad (4)$$

In this framework, each agent  $i$  first encodes sensor data  $X_i^t$  into features  $F_i^t$  via an encoder  $f_{\text{encoder}}$ . After transmission, these features arrive at the ego vehicle with a delay  $\tau$  and are transformed via coordinate transformation  $\xi_{i \rightarrow \text{ego}}^{t-\tau}$  to its coordinate frame, resulting in  $\hat{F}_{i \rightarrow \text{ego}}^{t-\tau}$ . The set of all such received features at each timestep is denoted as  $F_{\text{fused}}^{t-\tau}$ . As illustrated in Figure 2, CATNet then fuses these aligned features with the ego’s local historical features through three modules. Specifically, it utilizes a temporal alignment module to resolve asynchrony and a dual-stage denoising mechanism to suppress distortions, thereby producing fused features  $\tilde{F}_{\text{fused}}^t$ . Finally, a decoder  $f_{\text{decoder}}$  generates perception outputs  $\tilde{Y}_{\text{fused}}^t$ .

#### 3.2. Spatio-Temporal Recurrent Synchronization

Spatio-Temporal Recurrent Synchronization (STSync) is designed to address latency alignment in multi-agent cooperative perception. As shown in Figure 3, it employs

a dynamic timestamp calibration mechanism to sequentially model inter-frame motion. This unique approach compensates for latency-induced feature misalignment, ultimately ensuring robust spatio-temporal coherence across asynchronous data streams.

For a scene with  $N$  agents, the ego vehicle receives delayed features  $F_{\text{agents}}^{t-\tau} \in \mathbb{R}^{N \times C \times H \times W}$ . These are first processed by a dual-stream multi-scale fusion module (Integration) to generate a unified representation:

$$F_{\text{fused}}^{t-\tau} = \mathcal{C}_3 (\text{Concat} [\mathcal{M}_p(F_{\text{agents}}^{t-\tau}), \mathcal{A}_p(F_{\text{agents}}^{t-\tau})]) \quad (5)$$

where  $\mathcal{C}_3$  denotes a 3D convolution,  $\mathcal{M}_p$  and  $\mathcal{A}_p$  represent global max and average pooling operations, respectively.

The ego vehicle maintains a feature buffer,  $\mathcal{B}$ , which stores the  $K$  most recently fused historical features. This sequence is represented as  $\mathcal{B} = (B_1, B_2, \dots, B_K)$ , where each element  $B_j$  corresponds to a feature map from a historical timestep, specifically  $F_{\text{fused}}^{t-\tau-K+j}$ .

To model the temporal dependencies within this feature buffer, we introduce the Time-Augmented Recurrent Unit (TARU). Its hidden state is initialized with the earliest feature,  $H_1 = B_1$ . The module then iteratively operates for each timestep  $i$  from 2 to  $K$ , using a zero-tensor  $B_0$  to handle the initial boundary condition. The operations at each step  $i$  are:

**Motion Prediction.** To capture temporal dynamics, a motion offset is predicted by observing the two preceding features.

$$\Delta B_i = \text{Conv} (\text{Concat} [B_{i-2}, B_{i-1}]) \quad (6)$$

**Feature Warping.** The offset is used to warp the previous feature via deformable convolution, producing a motion-aligned feature  $\hat{B}_i$ .

$$\hat{B}_i = \text{DeformConv} (B_{i-1}, \Delta B_i) \quad (7)$$

**State Fusion.** The aligned feature  $\hat{B}_i$  is fused with the previous hidden state  $H_{i-1}$  using the Spatio-Temporal Gate (ST-Gate). ST-Gate employs parallel spatial and channel attention mechanisms (detailed in *Appendix I*) to ensure an adaptive fusion. These pathways process the concatenated hidden state and warped feature, computing an adaptive gating coefficient  $\alpha_i$ . This coefficient dynamically balances the contribution of historical context ( $H_{i-1}$ ) and current motion-aligned information ( $\hat{B}_i$ ). The fusion is then performed as a weighted sum:

$$S_i = (1 - \alpha_i) \cdot H_{i-1} + \alpha_i \cdot \hat{B}_i \quad (8)$$

This method enables the model to intelligently weigh temporal memory against current observations.

**Feature Update.** This intermediate state  $S_i$  undergoes further refinement to update the hidden state  $H_i$ . The final

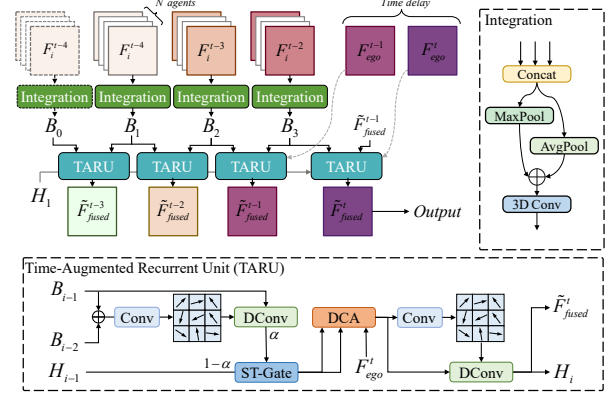


Figure 3. Architecture of the proposed STSync module. The module employs adaptive integration for preliminary multi-agent feature fusion, coupled with TARU that incorporates ego-vehicle features to achieve temporally coherent feature prediction.

hidden state  $H_K$  serves as the predicted feature.

$$H_i = \text{DeformConv} (\text{Conv} (S_i), S_i), \quad \tilde{F}_{\text{fused}}^t = H_K \quad (9)$$

Finally, this predicted feature  $\tilde{F}_{\text{fused}}^t$  is refined using Deformable Cross-Attention (DCA) with the ego-vehicle's own real-time feature  $F_{\text{ego}}^t$  as a spatial prior. This crucial step anchors the temporally-predicted features to the spatially accurate reality of the ego-vehicle, ensuring robust spatio-temporal alignment.

### 3.3. Dual-Branch Wavelet Enhanced Denoiser

Despite its effectiveness in feature synchronization, STSync still faces a persistent issue with residual artifacts, which primarily occur at the signal level: its iterative temporal processing can amplify high-frequency feature noise, and inherent inconsistencies between agents can corrupt local feature structures. To address these signal-level distortions, we introduce the Dual-Branch Wavelet Enhanced Denoiser (WTDen) as the first stage of our purification pipeline (Figure 4). WTDen operates in the wavelet domain, which allows it to isolate and suppress noise. Moreover, its dual-branch architecture enforces feature alignment on global and local scales.

The module first decomposes the fused feature map  $\tilde{F}_{\text{fused}}^t \in \mathbb{R}^{C \times H \times W}$  using the 2D Haar Wavelet Transform (WT). This process separates the spatial features into four subbands, each of dimension  $\in C \times \frac{H}{2} \times \frac{W}{2}$ .

$$F_{LL}, F_{LH}, F_{HL}, F_{HH} = \text{WT} \left( \tilde{F}_{\text{fused}}^t \right) \quad (10)$$

$F_{LL}$  captures the low-frequency structural information, while  $F_{LH}, F_{HL}, F_{HH}$  encode the high-frequency details.

**Wavelet Mamba.** This branch is designed to capture long-range spatial relationships and correct global feature

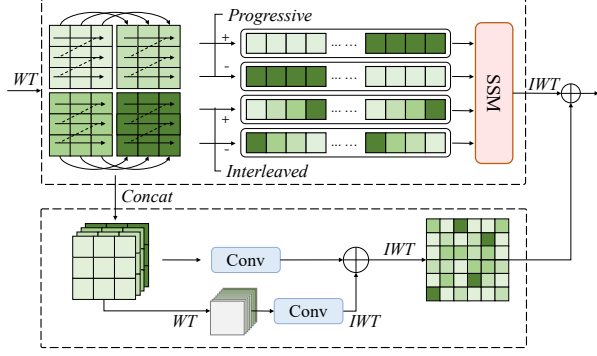


Figure 4. Architecture of the WTDen module. The module performs global and local feature denoising via a dual-branch design integrating wavelet-Mamba and wavelet convolution.

misalignment among agents. We employ a dual-path progressive fusion strategy within the Wavelet Mamba. One path is a forward integration that sequentially processes subbands from high-to-low frequency ( $F_{HH} \rightarrow F_{LL}$ ). This prioritizes high-frequency edge information to effectively compensate for detail loss. Concurrently, an interleaved scanning strategy processes features from all four subbands at each spatial location to capture cross-band correlations. Detailed illustration of scanning strategies is available in *Appendix.1*. The dual-path design incorporates reverse processes for both integration and scanning, ensuring comprehensive feature aggregation across all directions and scales. The outputs from four scanning paths ( $L_{\text{prog}}^{\pm}, L_{\text{inter}}^{\pm}$ ) are aggregated through SSM, and the resulting feature is processed to yield the four enhanced subbands:  $\{F_{LL}^{\text{fused}}, F_{LH}^{\text{fused}}, F_{HL}^{\text{fused}}, F_{HH}^{\text{fused}}\}$ . These are then fused via Inverse Wavelet Transform (IWT) to restore a globally aligned feature:

$$F_{\text{mam}} = \text{IWT}(\{F_{LL}^{\text{fused}}, F_{LH}^{\text{fused}}, F_{HL}^{\text{fused}}, F_{HH}^{\text{fused}}\}) \quad (11)$$

**Wavelet Convolution.** To complement the global alignment, this branch addresses local feature degradation and inconsistencies. It models fine-grained local patterns, ensuring that the features for each vehicle are coherent and free from localized noise. The four wavelet subbands are first concatenated, creating a tensor  $F_{\text{wt}} \in \mathbb{R}^{4C \times \frac{H}{2} \times \frac{W}{2}}$ . A hierarchical filtering process is then applied:

$$F_{\text{conv}} = \text{IWT}(\text{IWT}(\text{Conv}(\text{WT}(F_{\text{wt}}))) \oplus \text{Conv}(F_{\text{wt}})) \quad (12)$$

The final output combines both branch features:

$$F_{\text{denoise}} = F_{\text{mam}} + F_{\text{conv}} \quad (13)$$

### 3.4. Adaptive Feature Selector

The Adaptive Feature Selector (AdpSel) constitutes the second stage of synergistic purification, specifically designed

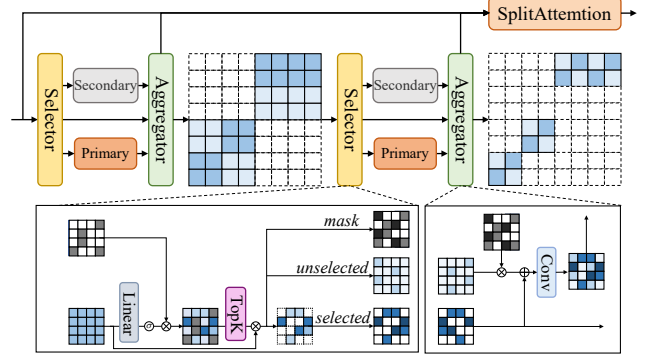


Figure 5. Architecture of the AdpSel module. The module divides features through a Selector, applies the MLLA module to enhance critical features, and employs inverted bottleneck convolution for feature compensation in non-critical regions. For critical features, these operations are iteratively applied, and the results are fused.

to address higher-order semantic artifacts that signal-level filters cannot remove. By redefining saliency as a proxy for semantic coherence, AdpSel performs context-aware synthesis to selectively enhance coherent feature regions, thereby filtering out semantic noise.

AdpSel operates iteratively across a set of predefined window scales  $\{S_1, S_2, \dots, S_n\}$ . As shown in Figure 5, the input feature map  $F_{\text{denoise}} \in \mathbb{R}^{N \times C \times H \times W}$  undergoes three key steps at each scale  $S_i$ :

**Coherence-Aware Block Selection.** The feature map is first partitioned into non-overlapping blocks  $F_{S_i}$ . A lightweight linear selector  $\phi(\cdot)$  assigns an importance score to each block, producing a score map  $\Phi_{S_i}$ . Based on these scores, we identify the top- $k\%$  of blocks as selected features ( $F_{S_i}^{\text{selected}}$ ) and the remainder as unselected features ( $F_{S_i}^{\text{unselected}}$ ). Let  $M_{S_i}^{\text{topk}} = \text{TopK}(\Phi_{S_i})$  be the binary mask for the top- $k$  blocks, then:

$$F_{S_i}^{\text{selected}} = M_{S_i}^{\text{topk}} \odot F_{S_i} \quad (14)$$

$$F_{S_i}^{\text{unselected}} = (1 - M_{S_i}^{\text{topk}}) \odot F_{S_i} \quad (15)$$

**Hierarchical Mask Refinement.** A key innovation of AdpSel is its cross-scale mask propagation. Low-saliency regions discarded at a finer scale  $S_i$  are used to refine the selection mask for the next, coarser scale  $S_{i+1}$ . Specifically, the mask of discarded regions ( $1 - M_{S_i}^{\text{topk}}$ ) is upsampled and integrated into the initial mask for the subsequent stage. This ensures that the model progressively focuses on globally salient areas while avoiding redundant computation on regions already identified as unimportant.

$$\text{mask}_{S_{i+1}} = \text{mask}_{\text{initial}} - \text{UpSample}(1 - M_{S_i}^{\text{topk}}) \quad (16)$$

**Dual-Path Feature Enhancement.** To maximize robustness, features are processed through a dual-path archi-

Table 1. Comparative evaluation of detection accuracy and model parameters with state-of-the-art methods on OPV2V, V2XSet, and DAIR-V2X datasets under latency and noise conditions. AP@0.5 and AP@0.7 metrics are presented separately. \*Regular methods. †Noise-robust methods. ‡Latency-aware methods.

Method	Published	Params	OPV2V		V2XSet		DAIR-V2X	
			AP@0.5	AP@0.7	AP@0.5	AP@0.7	AP@0.5	AP@0.7
No Fusion	–	–	0.738	0.509	0.698	0.516	0.625	0.446
*Where2comm [13]	NIPS’22	11.43 M	0.699	0.402	0.757	0.495	0.654	0.502
*CoMamba [17]	Arxiv’24	<b>09.15</b> M	0.743	0.558	0.726	0.531	0.635	0.479
†V2X-ViT [28]	ICRA’22	13.50 M	0.817	0.633	0.797	0.593	0.696	0.517
†CORE [26]	ICCV’23	09.19 M	0.831	0.628	0.764	0.504	–	–
†CoAlign [21]	ICRA’23	11.43 M	0.713	0.526	0.786	0.581	0.693	0.549
†DSRC [38]	AAAI’25	40.64 M	0.789	0.653	0.801	0.596	0.702	0.559
‡How2comm [32]	NIPS’23	35.80 M	0.739	0.562	0.749	0.624	0.624	0.472
‡ERMVP [37]	CVPR’24	12.42 M	0.820	0.679	0.744	0.499	0.674	0.554
‡MRCNet [11]	CVPR’24	19.71 M	0.814	0.617	0.817	0.618	0.665	0.539
<b>CATNet</b>	–	09.95 M	<b>0.843</b>	<b>0.686</b>	<b>0.858</b>	<b>0.643</b>	<b>0.723</b>	<b>0.565</b>

texture based on their semantic confidence score. The high-coherence selected blocks ( $F_{S_i}^{\text{selected}}$ ) are processed by the MLLA module [8] to capture complex contexts.

$$F_{S_i}^{\text{enhanced}} = \text{MLLA} (F_{S_i}^{\text{selected}}) \quad (17)$$

Concurrently, the unselected blocks ( $F_{S_i}^{\text{unselected}}$ ) are processed by a lightweight Inverted Bottleneck (IB) layer [20] to efficiently recover supplementary information with minimal overhead.

$$F_{S_i}^{\text{recovered}} = \text{IB} (F_{S_i}^{\text{unselected}}) \quad (18)$$

Finally, at each scale, an Aggregator module fuses the enhanced and recovered features via simple convolutions to produce a scale-specific output  $F_{S_i}^{\text{fused}}$ . After iterating through all scales, the resulting feature set  $\{F_{S_1}^{\text{fused}}, \dots, F_{S_n}^{\text{fused}}\}$  is fused by a SplitAttention [28] layer to generate the final output  $F_{\text{out}}$ .

$$F_{S_i}^{\text{fused}} = \text{Aggregator} (F_{S_i}^{\text{enhanced}}, F_{S_i}^{\text{recovered}}) \quad (19)$$

$$F_{\text{out}} = \text{SplitAttention} (F_{S_1}^{\text{fused}}, F_{S_2}^{\text{fused}}, \dots, F_{S_n}^{\text{fused}}) \quad (20)$$

## 4. Experiments

### 4.1. Experimental Setup

**Datasets and Metrics.** We comprehensively evaluate our proposed CATNet on three large-scale public benchmarks for cooperative perception: OPV2V [29], the first large-scale vehicle-to-vehicle dataset; V2XSet [28], the first vehicle-to-infrastructure dataset; and DAIR-V2X [36], a real-world dataset that captures complex and challenging scenarios. For a fair comparison, all methods use the standard PointPillar [15] backbone and are evaluated using the official Average Precision (AP) at IoU of 0.5 and 0.7.

**Comparison Methods.** We compare CATNet against a range of state-of-the-art approaches, categorized by their primary strength: regular methods (e.g., Where2comm [13]), noise-robust methods (e.g., V2X-ViT [28], DSRC [38]), and latency-aware methods (e.g., ERMVP [37], MRCNet [11]). We choose the naive intermediate method as the baseline. Further details are provided in *Appendix.1*.

### 4.2. Quantitative Results

**Detection Performance Analysis.** As quantified in Table 1, our method (CATNet) achieves consistent superiority across all evaluation metrics. Specifically, on the OPV2V dataset, our model achieves improvements of 1.2% / 0.7% in the key metrics of AP@0.5/AP@0.7, respectively, compared to the second-best model. On the V2XSet dataset, the performance gap is even more pronounced, with improvements of 4.1% / 1.9% in AP@0.5/AP@0.7. Similarly, on the DAIR-V2X dataset, our model outperforms the second-best model by 2.1% / 0.6% in these metrics. These results demonstrate that our model can achieve more accurate multi-vehicle object detection in complex vehicular environments.

**Noise Robustness Evaluation.** Figure 6 systematically demonstrates the robustness of CATNet through controlled noise injection experiments. By introducing heading perturbations (reflecting model parameter variations) and location offsets (emulating transmission interference), we simulate real-world noise conditions. Taking OPV2V as the representative case, two key observations emerge: 1) Progressive performance degradation in baseline methods under escalating noise intensities, with maximum AP@0.7 degradation of 7.98%/10.02% in heading and positional noise; 2) CATNet maintains consistent accuracy with only a 0.6% degradation in AP@0.7, demonstrating effective suppression of types of noise sources: spatial misalignment caused

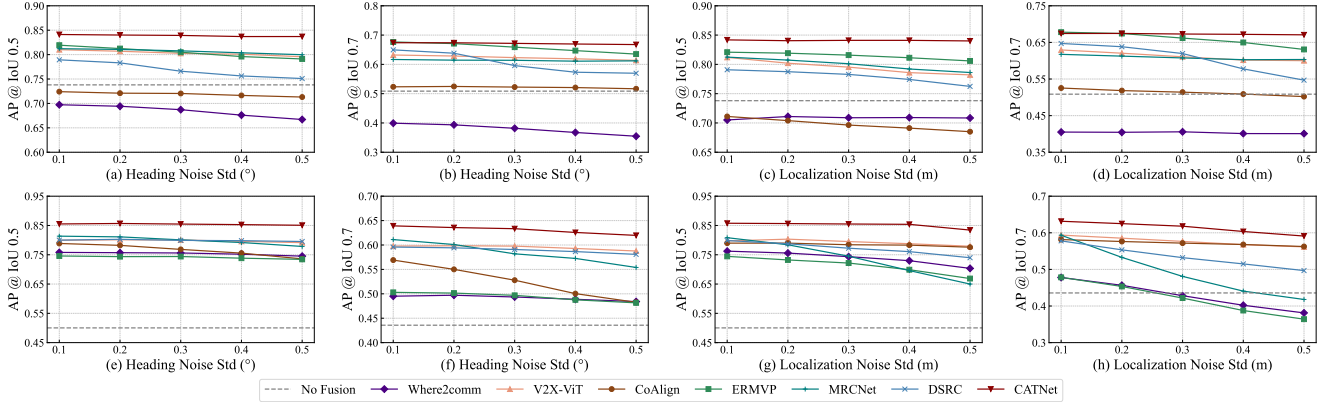


Figure 6. Quantitative analysis of noise robustness measured by AP@0.5/0.7: across OPV2V and V2XSet datasets; upper panels depict OPV2V performance, lower panels show V2XSet performance.

Table 2. Evaluation of methods under varying delay conditions on the OPV2V dataset.

Method	0ms		0-200ms		0-300ms		0-400ms		0-500ms	
	AP@0.5	AP@0.7								
CoAlign	0.881	0.748	0.709	0.517	0.658	0.524	0.631	0.508	0.610	0.495
V2X-ViT	0.863	0.724	0.774	0.580	0.738	0.557	0.716	0.538	0.697	0.530
ERMVP	0.831	0.686	0.824	0.643	0.783	0.630	0.767	0.613	0.745	0.600
MRCNet	0.848	0.715	0.836	0.647	0.774	0.638	0.759	0.625	0.738	0.615
DSRC	0.887	0.752	0.841	0.598	0.731	0.552	0.709	0.522	0.640	0.508
CATNet	<b>0.896</b>	<b>0.763</b>	<b>0.856</b>	<b>0.673</b>	<b>0.806</b>	<b>0.657</b>	<b>0.774</b>	<b>0.638</b>	<b>0.756</b>	<b>0.624</b>

by transmission noise while mitigating vehicle heading deviations induced by model parameter sensitivity.

**Latency Robustness Evaluation.** We assess latency robustness by subjecting methods to progressively harsher asynchronous conditions on OPV2V. For each condition, collaborators are perturbed with pose noise ( $\sigma = 0.2/0.2$ ) and a random latency drawn from a uniform distribution  $U[0, L]$ , where we systematically increase the maximum latency  $L$  from 200ms to 500ms. The results in Table 2 show that while performance degrades universally with increasing  $L$ , CATNet maintains a significant performance advantage across all conditions. This demonstrates the effectiveness of our temporal synchronization mechanism and validates the robustness against unpredictable delays.

### 4.3. Ablation Studies and Analysis

**Effectiveness of Core Components.** We conducted a comprehensive ablation study to evaluate the contribution of each core component across three datasets. We select the standard intermediate method [29] as our baseline. As presented in Table 3, all three modules consistently enhanced detection accuracy. Notably, STSync delivered the most significant improvements. For instance, it achieved gains of 22.3% and 2.4% in AP@0.5 compared to the baseline on the OPV2V and DAIR-V2X datasets, respectively. The

Table 3. Performance comparison of different module combinations on the OPV2V and DAIR-V2X datasets. This ablation study demonstrates the effectiveness of each proposed component.

Configuration	OPV2V	DAIR-V2X
Baseline	0.595/0.384	0.659/0.461
+ STSync	0.818/0.678	0.683/0.496
+ WTDen	0.645/0.461	0.671/0.482
+ AdpSel	0.624/0.425	0.666/0.477
+ STSync + WTDen	0.834/0.680	0.717/0.549
+ STSync + AdpSel	0.822/0.682	0.708/0.553
CATNet	<b>0.843/0.686</b>	<b>0.723/0.565</b>

final integrated CATNet model exhibited overall accuracy gains of 24.8% and 6.4% in AP@0.5 over the baseline.

**Robustness to Incomplete Historical Data.** To evaluate robustness against information loss, we simulated communication outages by randomly dropping a portion of data packets received from collaborators within a historical time window (e.g., 600ms). Results in Figure 7 reveal that the model maintained strong performance even under extreme conditions. On OPV2V, the performance consistently remained above 78%, and on V2XSet, the model still achieved over 65.0% AP@0.5 even under delays of up to

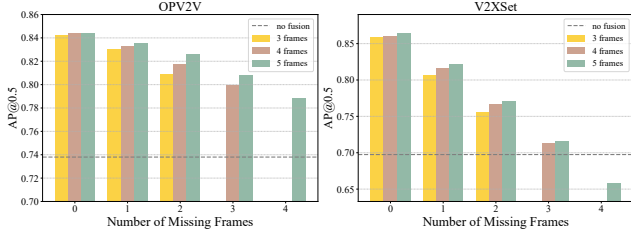


Figure 7. Comparison of STSync under historical data loss.

Table 4. Performance comparison of AdpSel with varying configuration ratios on the OPV2V, V2XSet, and DAIR-V2X datasets.

Proportion	OPV2V	V2XSet	DAIR-V2X
0.1	0.854/0.674	0.873/0.717	0.767/0.589
0.2	0.854/0.674	0.873/0.716	0.774/0.587
<b>0.3</b>	<b>0.855/0.691</b>	<b>0.874/0.717</b>	<b>0.775/0.603</b>
0.4	0.854/0.675	0.873/0.716	0.773/0.604
0.5	0.845/0.681	0.863/0.711	0.770/0.605
0.6	0.836/0.663	0.863/0.702	0.765/0.596

Table 5. AdpSel performance with block masking on OPV2V.

Module / Metric	AP@0.3	AP@0.5	AP@0.7
AdpSel	0.905	0.897	0.791
AdpSel (high mask)	0.366	0.364	0.328
AdpSel (low mask)	0.791	0.784	0.707

600ms. These results demonstrate that CATNet exhibits excellent robustness in edge scenarios with high latency.

**Token Retention Analysis.** Table 4 analyzes the effect of the token retention ratio ( $k\%$ ) in the standalone AdpSel module under ideal conditions. Results show that a 0.3 retention ratio achieves optimal performance on the dataset, emphasizing the critical role of optimal parameter selection in enhancing model accuracy.

**Effectiveness of AdpSel.** Table 5 demonstrates AdpSel’s impact by applying equal-intensity noise masks to high- and low-attention regions. The results show that masking high-attention areas significantly drops detection accuracy, confirming their critical role. Furthermore, the fusion of Primary and Secondary features achieves the highest feature reinforcement, which is vital for comprehensive perception. These findings highlight AdpSel’s effectiveness in guiding attention to salient features.

**Effectiveness of WTDen.** The WTDen module suppresses global noise from STSync by processing features in the wavelet domain. It simultaneously corrects feature misalignment via two branches: Wavelet Mamba uses our innovative hybrid scan to capture global positional relationships from frequency perspectives for alignment, while Wavelet Conv models local features to reduce inconsistencies. Table 6 demonstrates this module’s effectiveness. In delay-free

Table 6. Performance of Different Methods under Mixed Localization and Heading Noise

Method	0/0	0.2/0.2	0.4/0.4
Agent-graph	0.872/0.790	0.868/0.737	0.838/0.588
WTDen	0.893/0.795	0.875/0.737	0.860/0.654
FeaCo	0.881/0.784	0.874/0.755	0.855/0.649
CoAlign	0.888/0.790	0.881/0.748	0.848/0.633
DSRC	0.894/0.803	0.887/0.752	0.854/0.638
CATNet	0.905/0.807	0.896/0.763	0.870/0.663

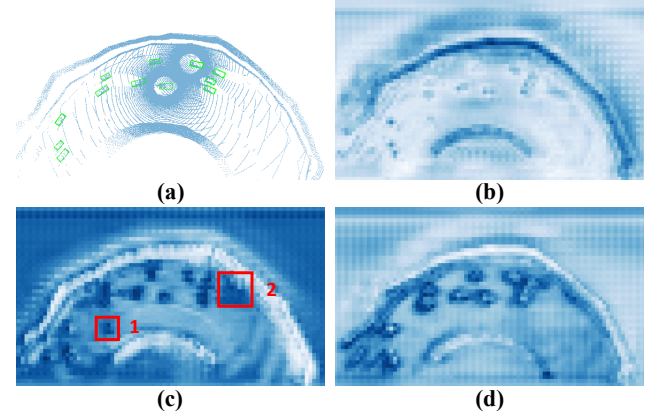


Figure 8. Heatmap comparison of collaborative perception performance. (a) Ground-truth. (b) Baseline. (c) CATNet (w/o WTDen). (d) CATNet (w/ WTDen).

scenarios with mixed localization and heading noise, CATNet surpasses existing noise-robust SOTA methods, especially under extreme conditions, confirming its crucial robustness for collaborative perception.

#### 4.4. Qualitative Results

Figure 8 visualizes the impact of WTDen through four cases. The proposed module significantly reduces artifacts in Regions 1-2 by synergistically mitigating both sensor noise and network-induced artifacts. The clearer denoised features in Figure 8 (d) further validate its ability to suppress interference while preserving structural semantics.

### 5. Conclusion

We investigate the issue of latency and noise in cooperative perception systems and propose a robust collaborative network, CATNet. This network first aligns asynchronous multi-vehicle features via a temporal recurrent module, then performs a comprehensive purification by first cleaning signal-level distortions and subsequently using semantic coherence to guide the final adaptive fusion. Results show that CATNet performs well in complex scenarios.

**Acknowledgement.** The work is supported in part by the S&T Program of Hebei Province (Beijing-Tianjin-Hebei

Collaborative Innovation Special Program) under Grant 25240701D.

## References

- [1] Eduardo Arnold, Mehrdad Dianati, Robert de Temple, and Saber Fallah. Cooperative perception for 3d object detection in driving scenarios using infrastructure sensors. *IEEE Transactions on Intelligent Transportation Systems (TITS)*, 23(3):1852–1864, 2022. 2
- [2] Gong Chen, Chaokun Zhang, Pengcheng Lv, and Xiaohui Xie. Cora: A collaborative robust architecture with hybrid fusion for efficient perception. *arXiv preprint arXiv:2512.13191*, 2025. 3
- [3] Gong Chen, Chaokun Zhang, and Pengcheng Lv. Coopdiff: A diffusion-guided approach for cooperation under corruptions, 2026. 3
- [4] Qi Chen, Sihai Tang, Qing Yang, and Song Fu. Cooper: Cooperative perception for connected autonomous vehicles based on 3d point clouds. In *International Conference on Distributed Computing Systems (ICDCS)*, pages 514–524, 2019. 2
- [5] Xin Gao, Xinyu Zhang, Yiguo Lu, Yuning Huang, Lei Yang, Yijin Xiong, and Peng Liu. A survey of collaborative perception in intelligent vehicles at intersections. *IEEE Transactions on Intelligent Vehicles (TIV)*, pages 1–20, 2024. 1
- [6] Jiaming Gu, Jingyu Zhang, Muiyang Zhang, Weiliang Meng, Shibiao Xu, Jiguang Zhang, and Xiaopeng Zhang. Feaco: Reaching robust feature-level consensus in noisy pose conditions. In *Proceedings of the ACM International Conference on Multimedia (ACM MM)*, pages 3628–3636, 2023. 1
- [7] Carl Gutwin, Steve Benford, Jeff Dyck, Mike Fraser, Ivan Vaghi, and Chris Greenhalgh. Revealing delay in collaborative environments. In *Proceedings of the SIGCHI Conference on Human Factors in Computing Systems*, pages 503–510, 2004. 2
- [8] Dongchen Han, Ziyi Wang, Zhuofan Xia, Yizeng Han, Yifan Pu, Chunjiang Ge, Jun Song, Shiji Song, Bo Zheng, and Gao Huang. Demystify mamba in vision: A linear attention perspective. In *Advances in Neural Information Processing Systems (NeurIPS)*, 2024. 6
- [9] Yushan Han, Hui Zhang, Huifang Li, Yi Jin, Congyan Lang, and Yidong Li. Collaborative perception in autonomous driving: Methods, datasets, and challenges. *IEEE Intelligent Transportation Systems Magazine*, 15(6):131–151, 2023. 1
- [10] Ruiyang Hao, Siqi Fan, Yingru Dai, Zhenlin Zhang, Chenxi Li, Yuntian Wang, Haibao Yu, Wenxian Yang, Jirui Yuan, and Zaiqing Nie. Rcooper: A real-world large-scale dataset for roadside cooperative perception. In *Proceedings of the IEEE/CVF Conference on Computer Vision and Pattern Recognition (CVPR)*, pages 22347–22357, 2024. 1
- [11] Shixin Hong, Yu Liu, Zhi Li, Shaohui Li, and You He. Mrcnet: Multi-agent collaborative perception via motion-aware robust communication network. In *Proceedings of the IEEE/CVF Conference on Computer Vision and Pattern Recognition (CVPR)*, pages 15301–15310, 2024. 2, 6
- [12] Senkang Hu, Zhengru Fang, Haonan An, Guowen Xu, Yuan Zhou, Xianhao Chen, and Yuguang Fang. Adaptive communications in collaborative perception with domain alignment for autonomous driving. In *IEEE Global Communications Conference (GLOBECOM)*, pages 746–751, 2024. 2
- [13] Yue Hu, Shaoheng Fang, Zixing Lei, Yiqi Zhong, and Siheng Chen. Where2comm: Communication-efficient collaborative perception via spatial confidence maps. *Advances in Neural Information Processing Systems (NeurIPS)*, 35: 4874–4886, 2022. 6
- [14] Zhe Huang, Shuo Wang, Yongcai Wang, Wanting Li, Deying Li, and Lei Wang. Roco: Robust cooperative perception by iterative object matching and pose adjustment. In *Proceedings of the ACM International Conference on Multimedia (ACM MM)*, pages 7833–7842, 2024. 2
- [15] Alex H Lang, Sourabh Vora, Holger Caesar, Lubing Zhou, Jiong Yang, and Oscar Beijbom. Pointpillars: Fast encoders for object detection from point clouds. In *Proceedings of the IEEE/CVF Conference on Computer Vision and Pattern Recognition (CVPR)*, pages 12697–12705, 2019. 6
- [16] Zixing Lei, Shunli Ren, Yue Hu, Wenjun Zhang, and Siheng Chen. Latency-aware collaborative perception. In *European Conference on Computer Vision (ECCV)*, pages 316–332, 2022. 2
- [17] Jinlong Li, Xinyu Liu, Baolu Li, Runsheng Xu, Jiachen Li, Hongkai Yu, and Zhengzhong Tu. Comamba: Real-time cooperative perception unlocked with state space models. *arXiv preprint arXiv:2409.10699*, 2024. 6
- [18] Xiang Li, Junbo Yin, Wei Li, Chengzhong Xu, Ruigang Yang, and Jianbing Shen. Di-v2x: Learning domain-invariant representation for vehicle-infrastructure collaborative 3d object detection. In *Proceedings of the AAAI Conference on Artificial Intelligence (AAAI)*, pages 3208–3215, 2024. 3
- [19] Yiming Li, Shunli Ren, Pengxiang Wu, Siheng Chen, Chen Feng, and Wenjun Zhang. Learning distilled collaboration graph for multi-agent perception. *Advances in Neural Information Processing Systems (NeurIPS)*, 34:29541–29552, 2021. 3
- [20] Zhuang Liu, Hanzi Mao, Chao-Yuan Wu, Christoph Feichtenhofer, Trevor Darrell, and Saining Xie. A convnet for the 2020s. In *Proceedings of the IEEE/CVF Conference on Computer Vision and Pattern Recognition (CVPR)*, pages 11976–11986, 2022. 6
- [21] Yifan Lu, Quanhao Li, Baoan Liu, Mehrdad Dianati, Chen Feng, Siheng Chen, and Yanfeng Wang. Robust collaborative 3d object detection in presence of pose errors. In *IEEE International Conference on Robotics and Automation (ICRA)*, pages 4812–4818, 2023. 2, 3, 6
- [22] Daniel Omeiza, Helena Webb, Marina Jirotko, and Lars Kunze. Explanations in autonomous driving: A survey. *IEEE Transactions on Intelligent Transportation Systems (TITS)*, 23(8):10142–10162, 2022. 1
- [23] Jing Pan, Hangguan Shan, Rongpeng Li, Yingxiao Wu, Weihua Wu, and Tony Q. S. Quek. Channel estimation based on deep learning in vehicle-to-everything environments. *IEEE Communications Letters*, 25(6):1891–1895, 2021. 1
- [24] Yucheng Sheng, Hao Ye, Le Liang, Shi Jin, and Geoffrey Ye Li. Semantic communication for cooperative perception

- based on importance map. *Journal of the Franklin Institute*, 361(6):106739, 2024. 2
- [25] Sanbao Su, Yiming Li, Sihong He, Songyang Han, Chen Feng, Caiwen Ding, and Fei Miao. Uncertainty quantification of collaborative detection for self-driving. In *IEEE International Conference on Robotics and Automation (ICRA)*, pages 5588–5594, 2023. 2
- [26] Binglu Wang, Lei Zhang, Zhaozhong Wang, Yongqiang Zhao, and Tianfei Zhou. Core: Cooperative reconstruction for multi-agent perception. In *Proceedings of the IEEE/CVF International Conference on Computer Vision (ICCV)*, pages 8710–8720, 2023. 6
- [27] Tsun-Hsuan Wang, Sivabalan Manivasagam, Ming Liang, Bin Yang, Wenyuan Zeng, and Raquel Urtasun. V2vnet: Vehicle-to-vehicle communication for joint perception and prediction. In *European Conference Computer Vision (ECCV)*, pages 605–621, 2020. 2
- [28] Runsheng Xu, Hao Xiang, Zhengzhong Tu, Xin Xia, Ming-Hsuan Yang, and Jiaqi Ma. V2x-vit: Vehicle-to-everything cooperative perception with vision transformer. In *Proceedings of the European Conference on Computer Vision (ECCV)*, 2022. 1, 2, 6
- [29] Runsheng Xu, Hao Xiang, Xin Xia, Xu Han, Jinlong Li, and Jiaqi Ma. Opv2v: An open benchmark dataset and fusion pipeline for perception with vehicle-to-vehicle communication. In *International Conference on Robotics and Automation (ICRA)*, pages 2583–2589, 2022. 1, 2, 6, 7
- [30] Runsheng Xu, Xin Xia, Jinlong Li, Hanzhao Li, Shuo Zhang, Zhengzhong Tu, Zonglin Meng, Hao Xiang, Xiaoyu Dong, Rui Song, et al. V2v4real: A real-world large-scale dataset for vehicle-to-vehicle cooperative perception. In *Proceedings of the IEEE/CVF Conference on Computer Vision and Pattern Recognition (CVPR)*, pages 13712–13722, 2023. 1
- [31] Runsheng Xu, Chia-Ju Chen, Zhengzhong Tu, and Ming-Hsuan Yang. V2x-vitv2: Improved vision transformers for vehicle-to-everything cooperative perception. *IEEE Transactions on Pattern Analysis and Machine Intelligence (TPAMI)*, 2024. 1
- [32] Dingkan Yang, Kun Yang, Yuzheng Wang, Jing Liu, Zhi Xu, Rongbin Yin, Peng Zhai, and Lihua Zhang. How2comm: Communication-efficient and collaboration-pragmatic multi-agent perception. *Advances in Neural Information Processing Systems (NeurIPS)*, 36:25151–25164, 2023. 2, 6
- [33] Kun Yang, Dingkan Yang, Jingyu Zhang, Mingcheng Li, Yang Liu, Jing Liu, Hanqi Wang, Peng Sun, and Liang Song. Spatio-temporal domain awareness for multi-agent collaborative perception. In *Proceedings of the IEEE/CVF International Conference on Computer Vision (ICCV)*, pages 23383–23392, 2023. 2
- [34] Melih Yazgan, Mythra Varun Akkanapragada, and J. Marius Zöllner. Collaborative perception datasets in autonomous driving: A survey. In *IEEE Intelligent Vehicles Symposium (IV)*, pages 2269–2276, 2024. 1
- [35] Melih Yazgan, Thomas Graf, Min Liu, Tobias Fleck, and J Marius Zöllner. A survey on intermediate fusion methods for collaborative perception categorized by real world challenges. In *IEEE Intelligent Vehicles Symposium (IV)*, pages 2226–2233, 2024. 1
- [36] Haibao Yu, Yizhen Luo, Mao Shu, Yiyi Huo, Zebang Yang, Yifeng Shi, Zhenglong Guo, Hanyu Li, Xing Hu, Jirui Yuan, and Zaiqing Nie. Dair-v2x: A large-scale dataset for vehicle-infrastructure cooperative 3d object detection. In *Proceedings of the IEEE/CVF Conference on Computer Vision and Pattern Recognition (CVPR)*, pages 21361–21370, 2022. 2, 6
- [37] Jingyu Zhang, Kun Yang, Yilei Wang, Hanqi Wang, Peng Sun, and Liang Song. Ermvp: Communication-efficient and collaboration-robust multi-vehicle perception in challenging environments. In *Proceedings of the IEEE/CVF Conference on Computer Vision and Pattern Recognition (CVPR)*, pages 12575–12584, 2024. 6
- [38] Jingyu Zhang, Yilei Wang, Lang Qian, Peng Sun, Zengwen Li, Sudong Jiang, Maolin Liu, and Liang Song. Dsrc: Learning density-insensitive and semantic-aware collaborative representation against corruptions. In *Proceedings of the AAAI Conference on Artificial Intelligence (AAAI)*, pages 9942–9950, 2025. 6
- [39] Chuyang Zhao, Yifan Sun, Wenhao Wang, Qiang Chen, Er-rui Ding, Yi Yang, and Jingdong Wang. Ms-detr: Efficient detr training with mixed supervision. In *Proceedings of the IEEE/CVF Conference on Computer Vision and Pattern Recognition (CVPR)*, pages 17027–17036, 2024. 2
- [40] Xizhou Zhu, Weijie Su, Lewei Lu, Bin Li, Xiaogang Wang, and Jifeng Dai. Deformable detr: Deformable transformers for end-to-end object detection. In *International Conference on Learning Representations (ICLR)*, 2021. 2